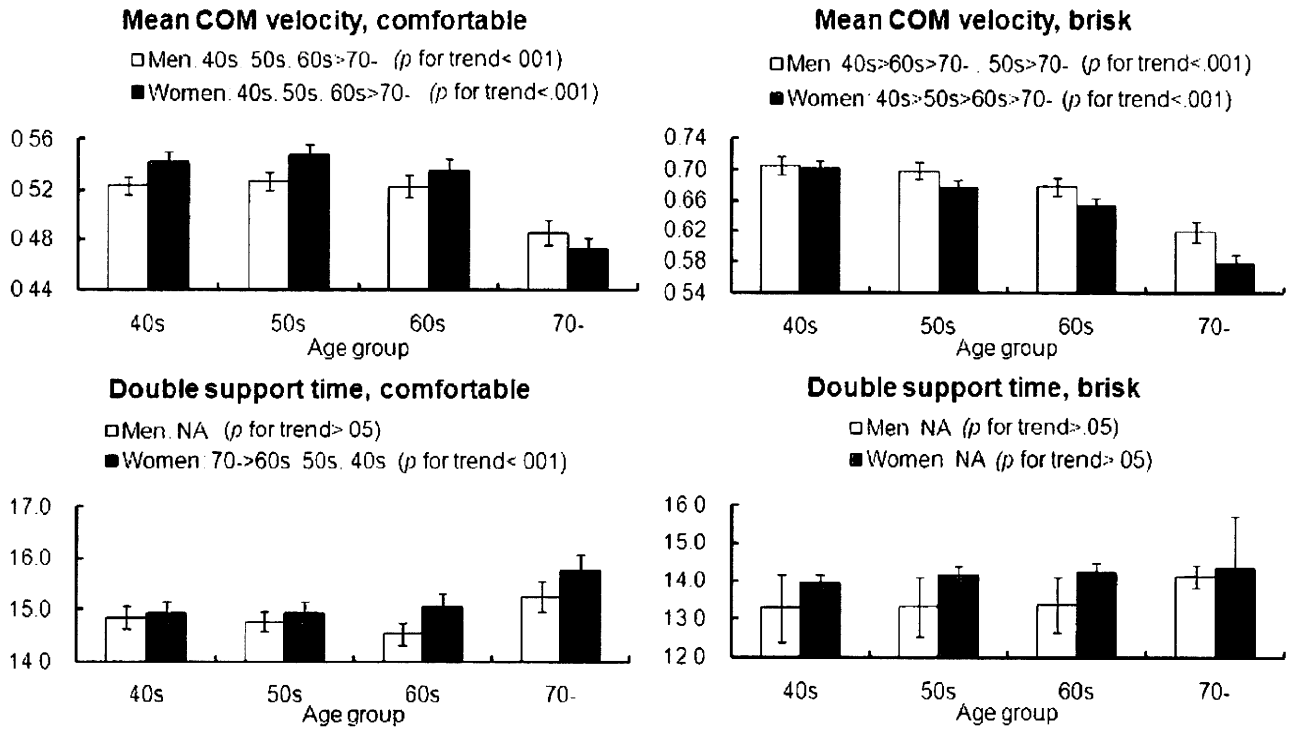

Figure 3 Age-related differences (trend tests and Tukey–Kramer tests); means and 95% confidence intervals of normalized mean center of mass (COM) velocities ($(m/sec)/\sqrt{((m/sec^2)\times m)}$) and double support times (s/s) during comfortable and brisk walking in men and women. Significant differences by age group in men and women are noted on the upper side of each figure. '>' indicates the significant difference between the age groups, with *P*-values of ≤0.05.

Table 4 Normalized mean COM velocities, step lengths and frequencies and double support times during comfortable and brisk walking among men and women

Walking parameters	Men				Women				*P*-value†
	N	Mean	SD	95% CI	N	Mean	SD	95% CI	
Comfortable walking									
Mean COM velocity	881	0.516	0.064	0.512–0.521	835	0.527	0.071	0.523–0.532	<0.001
Step length	982	0.889	0.083	0.883–0.894	944	0.886	0.085	0.881–0.891	NS
Step frequency	866	0.583	0.069	0.580–0.586	818	0.597	0.045	0.593–0.600	<0.001
Double support time (pre-swing)	839	14.8	1.7	14.7–14.9	763	15.1	1.8	15.0–15.2	<0.001
Brisk walking									
Mean COM velocity	798	0.677	0.089	0.671–0.683	816	0.656	0.089	0.650–0.662	<0.001
Step length	941	0.987	0.092	0.981–0.993	938	0.945	0.092	0.939–0.951	<0.001
Step frequency	756	0.687	0.075	0.682–0.692	794	0.698	0.049	0.693–0.703	<0.001
Double support time (pre-swing)	731	13.5	5.0	13.2–13.9	766	14.2	4.3	13.9–14.5	<0.01

†Student *t*-tests examine the sex differences. Values are numbers of samples (N), means, standard deviations (SD) and 95% confidence intervals (95% CI) at each variable. COM, center of mass; NS, not significant.

Further investigation should have discussed the difference between comfortable and brisk walking parameters.[38,42,43]

Age-related step length decreases during comfortable and brisk walking were almost concomitant with the COM velocity decreases, which was similar to the previous findings.[16,20] In brisk walking, however, age-related reduction in the step length seemed to be smaller than that in the step frequency compared with comfortable walking. For example, women's brisk step length decrease was 8.4% across middle-aged and elderly groups compared with their step frequency decrease of 10.7% (Table 3). This was observed also in men's. This may suggest that ambulatory ability observed in the COM velocity may be caused more by the step length during comfortable walking and the step frequency

during brisk walking in the elderly. This was also apparent in middle-aged women. The interpretation was limited qualitatively and should be further explored.

Step frequencies also decreased with age and this decrease was found even in middle-aged women during brisk walking. Previous studies in step frequency reported no age-related changes,[16,17,21] age-related decrease[8,18–20,25] and age-related increase.[26] Moreover, the current age- and sex-related decrease depending on required walking pace was not previously reported.[16,17] One explanation of these conflicts was that degree of the age-related reduction in step frequency was relatively less than that in other gait parameters such as velocity or step length.[8,17,19,20] Therefore, sample size, subject characteristics and measuring instruments may affect the age-related decrease in the step frequency.[16,25] Double support times in the present study did not increase with age, with the exception of women's comfortable data. On the other hand, exploratory analyses of actual values of double support times showed age-related increases in both sexes during both walking paces (data not shown, P for trend <0.001, <0.022). This shows that the double support as a percentage of one gait cycle remained almost constant in middle-aged and elderly subjects. Ferrandez *et al.*[32] found that double support time increased as velocity decreased, and that prolonged double support time was affected more by walking velocity than age.

The present study found brisk COM velocity and step length to be greater in men than in women. By contrast, step frequencies and double support times were greater in women than in men. This is characteristic of sex differences and is supported by previous findings.[8,17,21] Although the comfortable COM velocity was faster in women than in men, this is believed to be a result of the difference in body size as the actual comfortable COM velocity was significantly faster in men than in women (men, 1.46 ± 0.18 m/s; women, 1.43 ± 0.20 m/s; $P < 0.001$). The comfortable step length did not differ significantly between either sex group, perhaps because of the slower men's COM velocity.

The present gait data may give some insight into gait assessment and preventive walking exercise programs for older persons as previously reported.[42,44,45] The values for the gait parameters during one gait cycle may be useful to clinicians judging the ambulatory ability of patients from a short indoor walk.[7,42] Patients whose gait parameters are lower than that of their appropriate age group are at increased risk of ADL difficulties.[8,11] Comfortable and brisk walking velocities are predictive of adverse outcomes such as loss of physical function, requirement of caregivers, hospitalization and increased mortality in elderly persons.[8,10–12] Decreased step length and prolonged double support time are correlated with fear of falling and/or future fall risk.[4,5,9] Also, the other gait parameters such as gait velocity,[9,11] stride-to-stride variability[4] and lateral sway[3,5,6,46] are associated with the falling events. We did not directly ascertain whether the participants had a history of falls and/or a fear of falling in our gait parameters. Further work should confirm which gait measure is the best independent predictor for future fall risk in a large sample.

A moderate workload prescription in walking exercise programs should be given by controlling both step length and step frequency during comfortable walking in the elderly. Brisk walking, which is recommended for moderately vigorous endurance training and has a high impact compared to comfortable pace walking, might be considered for middle-aged women and the elderly to improve physical functions such as muscle strength[7,40,43] and/or cardiovascular fitness.[33,41]

This study has some limitations. Some previous gait investigations used the results of several trials or mean values of gait, while we used gait data from one trial of each participant. This was done because of technical difficulties in the automatically computed 3-D gait parameters. Next, the conjunction of our excluding criteria with the potential diseases might overestimate gait disorders: the elderly subjects were more likely to be healthy and physically fit. Moreover, patients with dementia were considered to be less in the present sample. The general comparability of the present gait variables with previously reported data is limited because of the lack of data for young adults in their 20s and 30s. Furthermore, our cross-sectional analysis approach could not demonstrate a cause-and-effect relationship from aging. We are planning longitudinal studies to further determine the effects of aging on gait. The present study included regional limitations such as race, culture, lifestyle, genetics and socioeconomic status which also may be important. However, the findings did permit age- and sex-related differences in gait to be clarified in the elderly.

In conclusion, age- and sex-related gait alterations were apparent in one gait cycle of walking in a large sample of community-dwelling, middle-aged and elderly Japanese men and women, when analyzed by a 3-D gait system. There were marked age-related gait differences in subjects aged 70 years and over compared to subjects aged 40–69 years during comfortable walking, and subtle differences were also observed in subjects aged 40–69 years during brisk walking. The earlier age-related changes were clearer in women than in men. These results may guide the assessment of gait patterns attributed to usual aging and to develop moderate exercise programs for the elderly.

Acknowledgments

The authors would like to thank the participants and their colleagues involved in the NILS-LSA. This study

was supported by a Grant-in-Aid for Exploratory Research from the Ministry of Education, Culture, Sports, Science and Technology of Japan (no. 18650203).

References

1 Bloem BR, Haan J, Lagaay AM, van Beek W, Wintzen AR, Roos RA. Investigation of gait in elderly subjects over 88 years of age. *J Geriatr Psychiatry Neurol* 1992; **5**: 78–84.
2 Marchetti GF, Whitney SL, Blatt PJ, Morris LO, Vance JM. Temporal and spatial characteristics of gait during performance of the Dynamic Gait Index in people with and people without balance or vestibular disorders. *Phys Ther* 2008; **88**: 640–651.
3 Tinetti ME, Speechley M, Ginter SF. Risk factors for falls among elderly persons living in the community. *N Engl J Med* 1988; **319**: 1701–1707.
4 Maki BE. Gait changes in older adults: predictors of falls or indicators of fear. *J Am Geriatr Soc* 1997; **45**: 313–320.
5 Barak Y, Wagenaar RC, Holt KG. Gait characteristics of elderly people with a history of falls: a dynamic approach. *Phys Ther* 2006; **86**: 1501–1510.
6 Chiba H, Ebihara S, Tomita N, Sasaki H, Butler JP. Differential gait kinematics between fallers and non-fallers in community-dwelling elderly people. *Geriatr Gerontol Int* 2005; **5**: 127–134.
7 Bohannon RW. Comfortable and maximum walking speed of adults aged 20–79 years: reference values and determinants. *Age Ageing* 1997; **26**: 15–19.
8 Callisaya ML, Blizzard L, Schmidt MD, McGinley JL, Srikanth VK. Sex modifies the relationship between age and gait: a population-based study of older adults. *J Gerontol A Biol Sci Med Sci* 2008; **63**: 165–170.
9 Verghese J, Holtzer R, Lipton RB, Wang C. Quantitative gait markers and incident fall risk in older adults. *J Gerontol A Biol Sci Med Sci* 2009; **64A**: 896–901.
10 Shinkai S, Watanabe S, Kumagai S *et al.* Walking speed as a good predictor for the onset of functional dependence in a Japanese rural community population. *Age Ageing* 2000; **29**: 441–446.
11 Montero-Odasso M, Schapira M, Soriano ER *et al.* Gait velocity as a single predictor of adverse events in healthy seniors aged 75 years and older. *J Gerontol A Biol Sci Med Sci* 2005; **60A**: 1304–1309.
12 Krishnamurthy M, Verghese J. Gait characteristics in nondisabled community-residing nonagenarians. *Arch Phys Med Rehabil* 2006; **87**: 541–545.
13 Verghese J, LeValley A, Hall CB, Katz MJ, Ambrose AF, Lipton RB. Epidemiology of gait disorders in community-residing older adults. *J Am Geriatr Soc* 2006; **54**: 255–261.
14 Berlau DJ, Corrada MM, Kawas C. The prevalence of disability in the oldest-old is high and continues to increase with age: findings from The 90+ Study. *Int J Geriatr Psychiatry* 2009; **24**: 1217–1225.
15 Demura S, Yamada T, Shin S. Age and sex differences in various stepping movements of the elderly. *Geriatr Gerontol Int* 2008; **8**: 180–187.
16 Oberg T, Karsznia A, Oberg K. Basic gait parameters: reference data for normal subjects, 10–79 years of age. *J Rehabil Res Dev* 1993; **30**: 210–223.
17 Auvinet B, Berrut G, Touzard C *et al.* Reference data for normal subjects obtained with an accelerometric device. *Gait Posture* 2002; **16**: 124–134.
18 Murray MP, Kory RC, Clarkson BH. Walking patterns in healthy old men. *J Gerontol* 1969; **24**: 169–178.
19 Himann JE, Cunningham DA, Rechnitzer PA, Peterson DB. Age-related changes in speed of walking. *Med Sci Sports Exerc* 1988; **20**: 161–166.
20 Kaneko M, Morimoto Y, Kimura M, Fuchimoto K, Fuchimoto T. A kinematic analysis of walking and physical fitness testing in elderly women. *Can J Sports Sci* 1991; **16**: 223–228.
21 Blanc Y, Balmer C, Landis T, Vingerhoets F. Temporal parameters and patterns of the foot roll over during walking: normative data for healthy adults. *Gait Posture* 1999; **10**: 97–108.
22 Winter DA. *Biomechanics and Motor Control of Human Movement*, 2nd edn. New York: John Wiley and Sons, 1991.
23 Pai Y-C, Patton J. Center of mass velocity-position predictions for balance control. *J Biomech* 1997; **30**: 347–354.
24 Riley PO, Della Croce U, Kerrigan DC. Effect of age on lower extremity joint moment contributions to gait speed. *Gait Posture* 2001; **14**: 264–270.
25 Prince F, Corriveau H, Hebert R, Winter DA. Gait in the elderly. *Gait Posture* 1997; **5**: 128–135.
26 Judge JO, Ounpuu S, Davis RB. Effects of age on the biomechanics and physiology of gait. *Clin Geriatr Med* 1996; **12**: 659–678.
27 Jansen EC, Vittas D, Helberg S, Hansen J. Normal gait of young and old men and women Ground reaction force measurement on a treadmill. *Acta Orthop Scand* 1982; **53**: 193–196.
28 Shimokata H, Ando F, Niino N. A new comprehensive study on aging – National Institute for Longevity Sciences, Longitudinal Study of Aging (NILS-LSA). *J Epidemiol* 2000; **10** (1 Suppl): S1–S9.
29 Kozakai R, Tsuzuku S, Yabe K, Ando F, Niino N, Shimokata H. Age-related changes in gait velocity and leg extension power in middle-aged and elderly people. *J Epidemiol* 2000; **10** (1 Suppl): S77–S81.
30 Perry J. *Gait Analysis: Normal and Pathological Function*. Thorofare, NJ: Slack, Inc., 1992.
31 Dobbs RJ, Charlett A, Bowes SG *et al.* Is this walk normal? *Age Ageing* 1993; **22**: 27–30.
32 Ferrandez A-M, Pailhouse J, Durup M. Slowness in elderly gait. *Exp Ageing Res* 1990; **16**: 79–89.
33 Tully MA, Cupples ME, Chan WS, McGlade K, Young IS. Brisk walking, fitness, and cardiovascular risk: a randomized controlled trial in primary care. *Prev Med* 2005; **41**: 622–628.
34 Clinical Gait Analysis Forum of Japan. *DIFF Manual*, ver. 1992.06, 1999.
35 Chandler RF, Clauser CE, McConville JT, Reynolds HM, Young JW. *Investigation of Inertial Properties of the Human Body*. Technical Report AMRL-TR-74-137. Dayton, OH: Wright-Patterson Air Force Base, 1975.
36 SAS Institute. *Base SAS 9.1.3 Procedures Guide*. Cary, NC: SAS Institute, 2006.
37 Hof AL. Scaling gait data to body size. *Gait Posture* 1996; **4**: 222–223.
38 Graham JE, Ostir GV, Kuo YF, Fisher SR, Ottenbacher KJ. Relationship between test methodology and mean velocity in timed walk tests: a review. *Arch Phys Med Rehabil* 2008; **89**: 865–872.
39 Liu MQ, Anderson FC, Schwartz MH, Delp SL. Muscle contributions to support and progression over a range of walking speeds. *J Biomech* 2008; **41**: 3243–3252.
40 Goldberg EJ, Neptune RR. Compensatory strategies during normal walking in response to muscle weakness and increased hip joint stiffness. *Gait Posture* 2007; **25**: 360–367.

41 Fleg JL, Morrell CH, Bos AG *et al.* Accelerated longitudinal decline of aerobic capacity in healthy older adults. *Circulation* 2005; **112**: 674–682.
42 Dobkin BH. Short-distance walking speed and timed walking distance: redundant measures for clinical trials? *Neurology* 2006; **66**: 584–586.
43 Kozakai R, Doyo W, Tsuzuku S *et al.* Relationships of muscle strength and power with leisure-time physical activity and adolescent exercise in middle-aged and elderly Japanese women. *Geriatr Gerontol Int* 2005; **5**: 182–188.
44 Oh-Park M, Zohman LR, Abraham C. A simple walk test to guide exercise programming of the elderly. *Am J Phys Med Rehabil* 1997; **76**: 208–212.
45 Morris JN, Hardman AE. Walking to health. *Sports Med* 1997; **23**: 306–332.
46 Gabell BA, Nayak US. The effect of age on variability in gait. *J Gerontol* 1984; **39**: 662–666.

the FEBS Journal

Proteolytic processing regulates pathological accumulation in dentatorubral-pallidoluysian atrophy

Yasuyo Suzuki[1], Kimiko Nakayama[1], Naohiro Hashimoto[2] and Ikuru Yazawa[1]

1 Laboratory of Research Resources, Research Institute for Longevity Sciences, National Center for Geriatrics and Gerontology, Aichi, Japan
2 Department of Regenerative Medicine, Research Institute for Longevity Sciences, National Center for Geriatrics and Gerontology, Aichi, Japan

Keywords
atrophin-1; dentatorubral-pallidoluysian atrophy; DRPLA; DRPLA protein; neurodegeneration; polyglutamine

Correspondence
I. Yazawa, Laboratory of Research Resources, Research Institute for Longevity Sciences, National Center for Geriatrics and Gerontology, 35 Gengo, Morioka-cho, Obu-shi, Aichi 474-7511, Japan
Fax: +81 562 46 8319
Tel: +81 562 46 2311
E-mail: yazawa@nils.go.jp

(Received 27 July 2010, revised 9 September 2010, accepted 23 September 2010)

doi:10.1111/j.1742-4658.2010.07893.x

Dentatorubral-pallidoluysian atrophy is caused by polyglutamine (polyQ) expansion in atrophin-1 (ATN1). Recent studies have shown that nuclear accumulation of ATN1 and cleaved fragments with expanded polyQ is the pathological process underlying neurodegeneration in dentatorubral-pallidoluysian atrophy. However, the mechanism underlying the proteolytic processing of ATN1 remains unclear. In the present study, we examined the proteolytic processing of ATN1 aiming to understand the mechanisms of ATN1 accumulation with polyQ expansion. Using COS-7 and Neuro2a cells that express the *ATN1* gene, in which ATN1 was accumulated by increasing the number of polyQs, we identified a novel C-terminal fragment containing a polyQ tract. The mutant C-terminal fragment with expanded polyQ selectively accumulated in the cells, and this was also demonstrated in the brain tissues of patients with dentatorubral-pallidoluysian atrophy. Immunocytochemical and biochemical studies revealed that full-length ATN1 and C-terminal fragments displayed individual localization. The mutant C-terminal fragment was preferentially found in the cytoplasmic membrane/organelle and insoluble fractions. Accordingly, it is assumed that the proteolytic processing of ATN1 regulates the localization of C-terminal fragments. Accumulation of the C-terminal fragment was enhanced by inhibition of caspases in the cytoplasm of COS-7 cells. Collectively, these results suggest that the C-terminal fragment plays a principal role in the pathological accumulation of ATN1 in dentatorubral-pallidoluysian atrophy.

Introduction

The polyglutamine (polyQ) diseases are a group of hereditary neurodegenerative disorders that include Huntington's disease (HD), dentatorubral-pallidoluysian atrophy (DRPLA), spinal and bulbar muscular atrophy, and several forms of spinocerebellar ataxia [1–3]. These diseases are caused by expansion of CAG trinucleotide repeats that encode a polyQ tract in the responsible genes. Aside from the CAG trinucleotide repeat, the genes responsible for the various polyQ diseases have no homology to one other. Therefore, speculation concerning the pathogenesis has been focused on the expanded polyQ itself, which appears to cause the gene products to undergo a conformational change that makes them aggregate in neurones [4]. This

Abbreviations
ALLN, *N*-acetyl-Leu-Leu-norleucinal; ATN1, atrophin-1; DRPLA, dentatorubral-pallidoluysian atrophy; GFP, green fluorescent protein; HD, Huntington's disease; HRP, horseradish peroxidase; NLS, nuclear localizing signal; polyQ, polyglutamine; TPEN, *N,N,N′,N′*-tetrakis(2-pyridylmethyl)ethylenediamine; TUNEL, terminal deoxynucleotidyl transferase-mediated dUTP nick end labelling; Z-VAD-FMK, benzyloxycarbonyl-Val-Ala-Asp(OMe)-fluoromethyl ketone.

finding suggests that the mechanism of pathogenesis is derived from aggregation of proteins or peptides with the expanded polyQ. By contrast, the onset of a neurological phenotype or cell dysfunction mediated by the expanded polyQ in the responsible gene product was independent of the formation of inclusions [5–7]. Indeed, a previous study showed that the presence of inclusion bodies reduced the risk of neuronal death as a result of polyQ expansion [8]. Thus, the relationship between inclusions and neurotoxicity remains controversial [9]. The polyQ diseases show progressive and refractory neurological symptoms that are caused by neuronal cell loss in selective regions of the central nervous system. This selective neuronal damage gives rise to the specific features of each disease. Accordingly, we hypothesized that each polyQ disease has a distinct molecular mechanism underlying its characteristic neurodegeneration.

DRPLA is an autosomal dominant neurodegenerative disorder characterized clinically by progressive dementia, epilepsy, gait disturbance and involuntary movement (chorea and myoclonus) and, pathologically, by combined degeneration of the dentatorubral and pallidoluysian systems [10,11]. DRPLA pedigrees show genetic anticipation and phenotypic heterogeneity [12–14]. DRPLA is caused by expansion of the polyQ tract within DRPLA protein, also known as atrophin-1 (ATN1). ATN1 is ubiquitously expressed in the central nervous system, although selective regions of the central nervous system are involved in the neuronal degeneration in DRPLA [15]. A previous study using cultured cells expressing ATN1 showed that truncated ATN1 with an expanded polyQ formed perinuclear and intranuclear aggregates and caused apoptotic cell death [16]. Cleavage of ATN1 may be relevant to the disease pathogenesis, although the nature of the relevant cleavage product is uncertain. Previous studies in a transgenic mice model and DRPLA patients have shown that a 120 kDa N-terminal fragment of mutant ATN1 accumulates within the nuclei of neurones [17,18]. On the other hand, we have previously reported evidence of an ~ 100 kDa C-terminal fragment in the normal control and DRPLA human brains [15]. Caspase cleavage of ATN1 at Asp109 generates a large C-terminal fragment [19–21], although whether the caspase cleavage occurs *in vivo* remains uncertain. In the present study, we report a novel C-terminal fragment of ATN1 that contains a polyQ tract found in cellular models of DRPLA, which expresses ATN1 and manifests accumulation of ATN1 with the expanded polyQ. Moreover, the novel C-terminal fragment with the expanded polyQ was discovered in the brain tissues of DRPLA patients. From these results, we hypothesize that pathological ATN1 accumulation underlies neurodegeneration in DRPLA.

Results

Construction of shortened and expanded CAG repeat of *ATN1* gene

The *ATN1* gene was fused to a His-tag and a T7-tag at the 5′-end, and to a *Strep*-tag II at the 3′-end (Fig. 1A). To produce mutant proteins with various numbers of glutamine repeats, we established a method for making the intended CAG repeat a stable PCR product. PCR was performed using oligonucleotides, 5′-$(CAG)_{10}$-3′ and its complementary strand, without DNA templates. The approximately required size of the CAG repeat was obtained by PCR with CAG/CTG oligomer (Fig. S1). The full-length mutant *ATN1* genes were prepared by cassette mutagenesis. The full-length cDNAs of ATN1 with different numbers of the CAG repeat were constructed; the numbers of the translated glutamine repeat are 0, 4, 19, 31, 47, 54 and 77 (Fig. 1B). The polyQ repeat size 0 is a deletion, 4 is shortened, 19 and 31 are normal, 47 is borderline, and 54 and 77 are in the abnormal range. Each expressed protein was represented by adding the number of glutamine repeats it includes after ATN1 (e.g. ATN1-Q19).

Expression of ATN1 in mammalian cells

The cloned cDNA of ATN1 encoded a 1190 amino acid protein that contains the normal 19 polyQ repeat (ATN1-Q19). ATN1 expression systems were constructed for COS-7 and Neuro2a cells. COS-7 and Neuro2a cells were transiently transfected with *ATN1-Q19*-pcDNA3.1 by lipofection. We detected cellular expression of ATN1s with ATN1 antibodies: L55-2 and C580R. Immunoblots of ATN1-Q19 expressed in COS-7 and Neuro2a cells revealed that the ATN1 antibodies labelled two C-terminal fragments of ATN1 with estimated molecular masses of 140 kDa (F1) and 125 kDa (F2), in addition to the full-length ATN1 (Figs 1C,D and S2). The T7-tag antibody detected only the full-length ATN1 at 165 kDa but no fragment (Fig. 1C). Immunoblots of ATN1-Q77 in COS-7 and Neuro2a cells also revealed that L55-2 and C580R recognized the full-length ATN1 at 185 kDa and two C-terminal fragments (Fig. 1C,D). These 160 and 145 kDa fragments corresponded with the mutant F1 fragment with expanded polyQ (mF1) and the mutant F2 fragment (mF2), respectively. The immunoblots of ATN1-Q19 and -Q77 also showed that an antibody

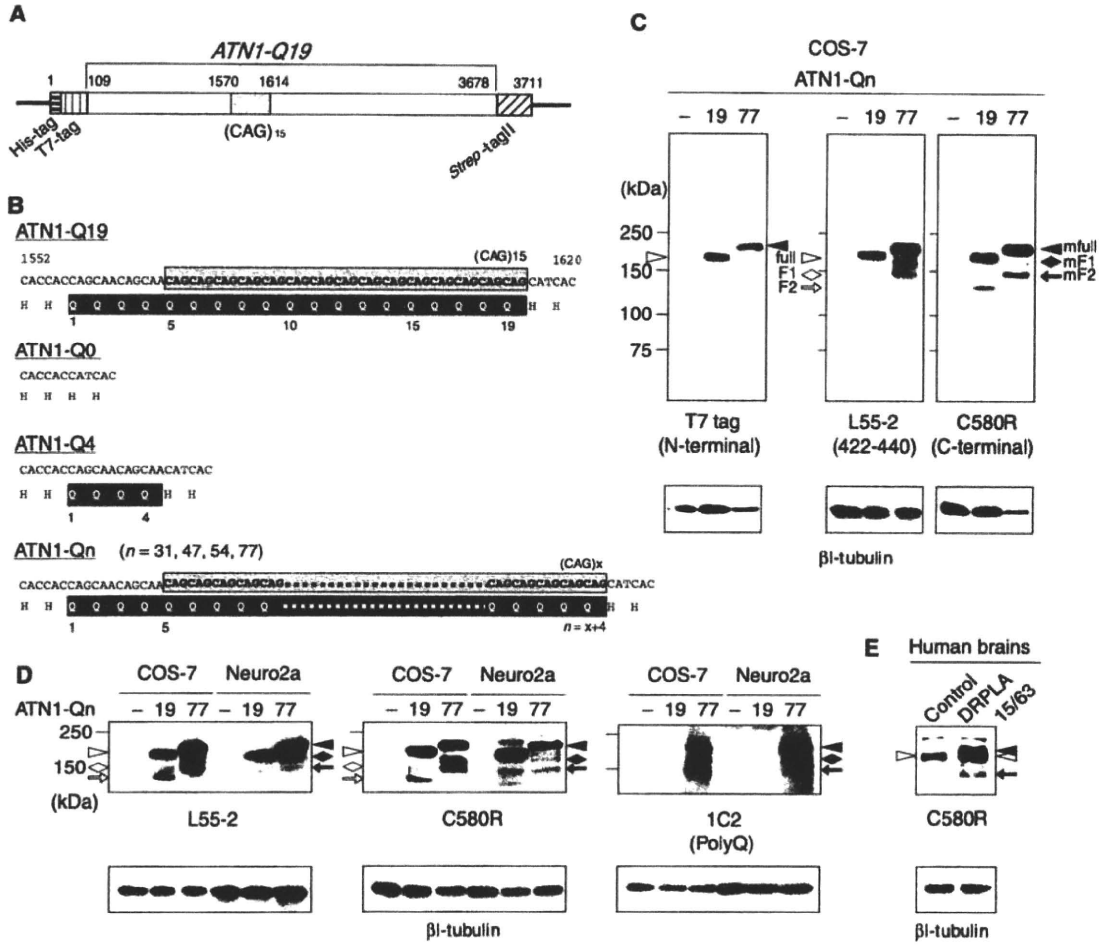

Fig. 1. (A) cDNA constructs of *ATN1* gene and expression of ATN1 in mammalian cells. The ORF of *ATN1-Q19* is shown in the box. The regions encoding the three tags are hatched and the CAG repeat is shown in grey. Numbers above the box represent the positions of the nucleotide counted from the initiation of the cDNA construct. (B) A series of polyQ regions of mutated ATN1 are illustrated. The nucleotides and their corresponding amino acid sequences around the CAG repeat are shown. The regions of CAG repeat in cDNA are shown in grey and the polyQ in the amino acid sequences is shown in black. (C) ATN1-Q19 and -Q77 were expressed in COS-7 cells. Expressed ATN1 was detected by immunoblotting using T7-tag, L55-2 and C580R antibodies. The immunoblots revealed that the full-length ATN1 was cleaved into two fragments containing the C-terminal and polyQ tract. The arrowheads show the full-length ATN1-Q19 (white) and full-length ATN1-Q77 (black). C-terminal fragments are defined as F1 (white lozenge) and F2 (white arrow). In ATN1-Q77, they are defined as mF1 (black lozenge) and mF2 (black arrow). βI-tubulin was examined as a loading control. (D) We expressed ATN1-Q19 and -Q77 in COS-7 and Neuro2a cells. ATN1s expression was compared using immunoblotting with ATN1 antibodies (C580R and L55-2) and polyQ antibody (1C2). The antibodies showed no difference in immunoreactivity of ATN1 and various fragments between the Neuro2a and COS-7 cells. 1C2 labelled the ATN1-Q77 bands but not the ATN1-Q19 band. βI-Tubulin was used as a loading control. Representative immunoblots of three independent experiments are shown. (E) Tissue samples of the cerebellum of a patient with DRPLA and the human control brain tissue were examined by immunoblotting. The antibody C580R recognized the C-terminal of ATN1 mutant (black arrowhead) and wild-type (white arrowhead), the full-length ATN1s in the DRPLA brain tissue. A novel C-terminal fragment mF2 with an expanded polyQ tract (black arrow) was identified in the DRPLA brain tissue.

against polyQ tracts, 1C2, detected the same immunoreactivity of ATN1 and fragments as L55-2 (Fig. 1D), which indicates that the C-terminal fragments of mF1 and mF2 contained polyQ tracts.

Furthermore, the brain tissues from DRPLA patients also contained the C-terminal fragment of ATN1 containing an expanded polyQ tract. Immunoblots of the brain tissues from DRPLA patients revealed an immunoreactive, C580R-labelled band at ~ 150 kDa, which corresponds with the results of mF2 fragment of ATN1-Q77 in COS-7 cells (Fig. 1E, black arrow). Taken together, these results demonstrated that the mutant, full-length ATN1 was cleaved into the C-terminal fragment of mF2 in the mammalian cultured cells and

human brains. Because immunoblots revealed apparently different amounts of the full-length ATN1 and C-terminal fragment proteins in ATN1-Q19 and -Q77 of the COS-7 expression, we performed a quantitative assessment of ATN1 expression by western blotting with *Strep*-Tactin horseradish peroxidase (HRP) conjugate.

Accumulation of ATN1 and C-terminal fragments with expansion of polyQ in COS-7 cells

To examine differential expression of ATN1 with varying numbers of polyQs, ATN1-Q0, -Q4, -Q19, -Q31, -Q47, -Q54 and -Q77 were overexpressed in COS-7 cells and *Escherichia coli*. We directly detected ATN1s with *Strep*-tag II expressed in the COS-7 cells and *E. coli* using western blotting with the *Strep*-Tactin HRP conjugate. Western blots of the expressed ATN1s in COS-7 cells showed that the reactivity of the full-length ATN1 and F2 bands increased with the increase of the polyQ size (Fig. 2A), whereas the blots of ATN1s in *E. coli* showed no difference in the reactivity of the full-length or fragmented ATN1s (Fig. 2B). Quantitative analyses of the blots confirmed the increased reactivity in COS-7 cells but not in *E. coli* (Fig. 2C,D). In addition, an immunocytochemical study of COS-7 cells expressing ATN1s showed an apparent increase in the immunoreactivity of ATN1 antibody with ATN1-Q77 compared to ATN1-Q19 (Fig. 2E). These data indicate that the amount of the full-length ATN1 and fragments increased in the COS-7 cells as the size of the polyQ was increased.

Next, we assessed whether the quantitative increase of the full-length ATN1 and fragments was the result of an accumulation caused by the prolonged life span of the proteins. We examined the stability of ATN1-Q19 and -Q77 by inhibition of protein synthesis. At each time point, equal amounts of protein were separated in gels, and these were examined by western blotting. We found that, after cycloheximide treatment, the protein levels of ATN1 and fragments were quickly decreased by degradation, whereas no reduction of βI-tubulin or green fluorescent protein (GFP) (controls) occurred (Fig. 3A). ATN1-Q77 and -Q19 exhibited significantly different speeds of degradation. Western blots showed that the full-length ATN1 decreased to ~ 70% at 30 min after treating ATN1-Q77 with cycloheximide, whereas the full-length ATN1-Q19 decreased to < 20% at 30 min (Fig. 3B). These results indicate the increase of ATN1 and fragments was a result of accumulation. Moreover, the mF2 fragment showed a smaller decrease than the mutant, full-length ATN1 and mF1 fragment in ATN1-Q77 at 30 min after treatment (Fig. 3C). Thus, the mF2 fragment is selectively accumulated by the expansion of the polyQ tract. We then investigated where mF2 accumulated in the cells.

Subcellular localization of ATN1 and fragments

Although previous immunohistological studies showed that ATN1 localized to both the nucleus and cytoplasm of neuronal cells [15,22,23], the precise intracellular localization of the ATN1 fragments remains unclear. To determine the intracellular localization of the full-length ATN1 and the C-terminal fragments, we first biochemically analyzed COS-7 cells that expressed ATN1 by subcellular fractionation using low-speed centrifugation. The COS-7 cells were fractionated into crude nuclear and non-nuclear fractions. Western blots of COS-7 expressing ATN1-Q19 revealed that the full-length ATN1 was located in the nuclear and non-nuclear fractions, although the C-terminal fragments were located only in the nuclear fraction (Fig. S3). Furthermore, western blots of COS-7 cells expressing ATN1-Q77 showed that the full-length ATN1 and the mF2 fragment were located in the nuclear and non-nuclear fractions. To further elucidate the intracellular localization of the full-length ATN1 and fragments, we performed subcellular fractionation of the proteins into four fractions: cytosol, cytoplasmic membrane/organelle, nucleus and insoluble. Western blots of ATN1-Q19 displayed reactivity of the full-length ATN1 and F2 in both the nuclear and insoluble fractions but F1 in the insoluble fraction only (Fig. 4A). Furthermore, western blots of ATN1-Q77 indicated mF2 was located in the membrane/organelle and insoluble fractions, in addition to the nuclear fraction (Fig. 4A). The mutant, full-length ATN1 and mF1 of ATN1-Q77 were observed in the same fractions as those of ATN1-Q19. The blotting data indicated that the F2 fragment was located in the nuclear and insoluble fractions of those ATN1s with a normal polyQ repeat size, whereas mF2 showed specific localization in the cytoplasmic membrane/organelle fraction in addition to the other fractions when the size of the polyQ tract was expanded. We immunocytochemically examined the COS-7 cells 24 h after transfection using His-tag antibody and C580R. Both antibodies showed diffuse nuclear staining and granular cytoplasmic staining (Fig. 4B). The ATN1-Q19 and -Q77 exhibited similar localization in the cytoplasm and nucleus. However, the immunoreactivity of ATN1-Q77 was stronger than that of ATN1-Q19. Taken together, these biochemical and immunocytochemical studies revealed that the full-length ATN1 and the fragments localized in the nucleus and in the cytoplasm, and that

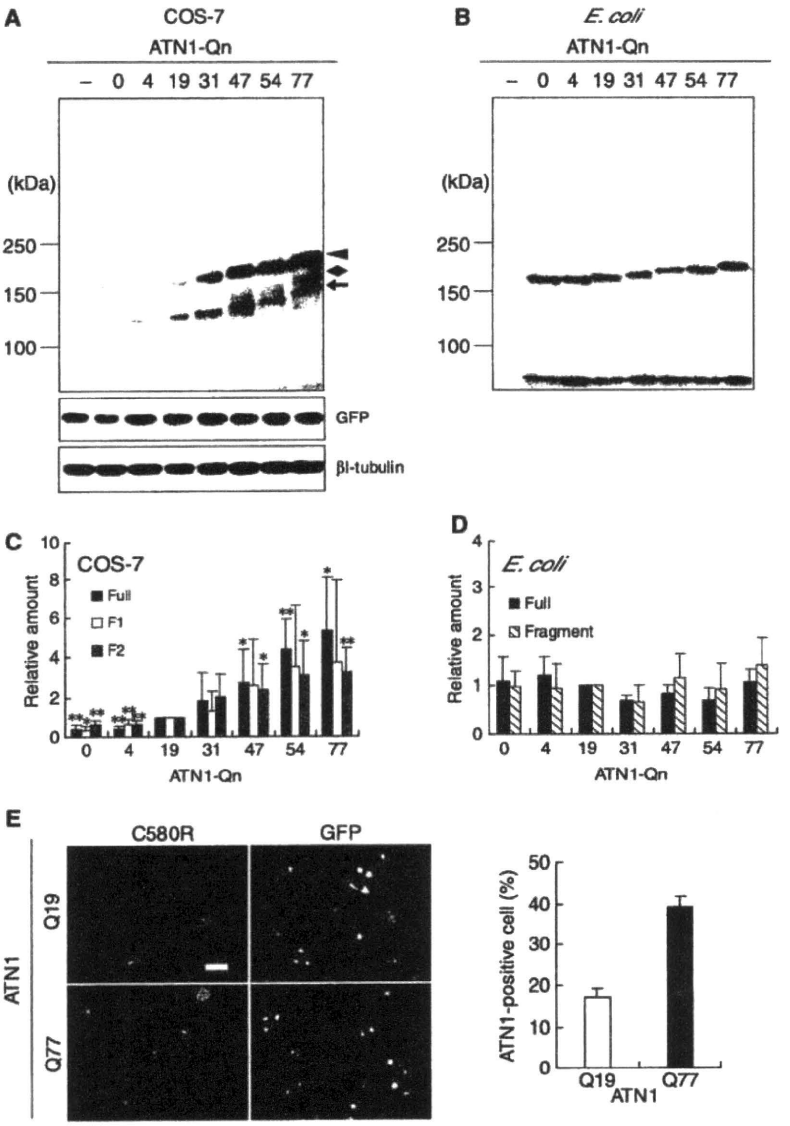

Fig. 2. Accumulation of ATN1 and fragments as a result of expanded polyQ in COS-7 cells. (A) Transiently expressed ATN1-Q0, -Q4, -Q19, -Q31, -Q47, -Q54 and -Q77 in COS-7 cells were examined by western blotting using *Strep*-Tactin HRP conjugate. Western blots showed that the reactivity of the full-length ATN1, F1 and F2 increased with the increase of polyQ size. GFP was used as a transfection control and βI-tubulin as a loading control. The arrowhead, lozenge and arrow indicate the full-length ATN1, F1 and F2, respectively. (B) ATN1s were expressed in *E. coli* Rosetta(DE3)pLysS. Western blotting showed no changes in the reactivity of the full-length ATN1 and C-terminal fragments with any polyQ size. (C) Quantification is presented as the relative ratio of the full-length ATN1 (black), F1 (white) and F2 (grey) to βI-tubulin in COS-7 cells. Densitometric measurement of the signals was performed using IMAGEJ software (US National Institutes of Health, Bethesda, MD, USA) and the intensities of the signals were expressed as relative values. The density is relative to each ATN1-Q19 peptide as the corresponding control. These data showed that the full-length ATN1 and F2 expression increased with the increase of polyQ size in COS-7 cells. $*P < 0.05$ and $**P < 0.01$ (Student's *t*-tests). The height of the columns indicates the relative amount and the error bars represent the SD ($n = 5$). (D) Relative quantification of signals of the full-length ATN1 (black) and a C-terminal fragment (stripe) of ATN1 from bacterial cells. Densitometric measurement of the signals showed that there was no quantitative difference among the ATN1s and fragments expressed in *E. coli* with any polyQ size. The density is relative to the full-length ATN1-Q19 protein as the control. The height of the columns indicates the relative amount and the error bars represent the SD ($n = 3$). (E) Twenty-four hours after transfection with the ATN1-Q19 or -Q77 construct, COS-7 cells were immunostained with ATN1 antibody C580R (left panels) or GFP antibody (right panels). C580R detected more ATN1 immunoreactivity in ATN1-Q77 than in ATN1-Q19, whereas GFP showed no significant difference between constructs. Scale bar = 100 μm. The bar graph shows the ratio of ATN1-positive cells to co-expressed GFP-positive cells, and error bars represent the SD ($n = 3$).

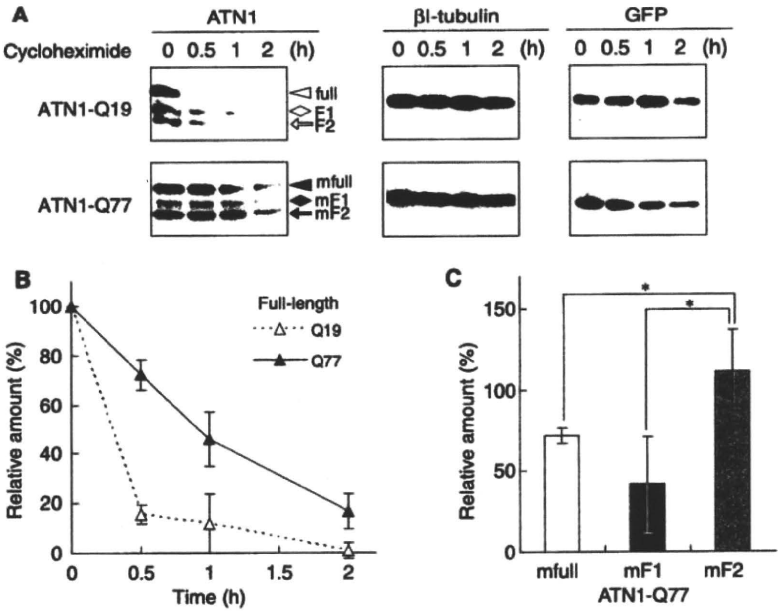

Fig. 3. Effect of polyQ size on stability of ATN1 peptides. (A) COS-7 cells transfected ATN1-Q19 and -Q77 were treated with 100 $\mu g \cdot mL^{-1}$ cycloheximide (at time 0), which blocks protein synthesis in eukaryotic cells. At the indicated time points, the cells were harvested as described in the Experimental procedures. Western blots showed that the full-length ATN1s and fragments were quickly decreased over time. (B) At all time points, the full-length ATN1-Q19 and -Q77 were quantitatively assessed on the western blots. The line graph shows that ATN1-Q77 was degraded more slowly than ATN1-Q19 in the cells. $*P < 0.05$ (Student's *t*-test). The points indicate the relative amount and the error bars represent the SD ($n = 3$). (C) Thirty minutes after treatment of ATN1-Q77, the mutant full-length, mF1 and mF2 levels were quantitatively assessed on the blots. The bar graph shows that the decrease in mF2 was less than those in the full-length ATN1 and mF1. Means data are plotted from four independent experiments. $*P < 0.05$ (Student's *t*-test). Error bars represent the SD.

the mF2 fragment with an expanded polyQ tract also localized in the membrane/organelle and insoluble fractions of the cytoplasm. Thus, expansion of the polyQ tract induces pathological accumulation of the mF2 fragment of ATN1 in the cytoplasm.

Furthermore, to explore the biological relevance of polyQ expansion in the ATN1s to cell toxicity, we performed terminal deoxynucleotidyl transferase-mediated dUTP nick end labelling (TUNEL) assays to detect nuclear fragmentation, which is a hallmark of apoptosis. TUNEL-staining showed that expression of ATN1-Q77 in Neuro2a cells induced apoptosis, whereas the expression of ATN1-Q19 resulted in no apoptosis (Fig. S4). These data suggest that ATN1 and fragments with expanded polyQ could cause neurotoxicity by the accumulation of mF2 in the cytoplasmic membrane/organelle fraction.

Cleavage of ATN1 into mF2 in the brain tissues of DRPLA patients

We next assessed the proteolytic processing of ATN1 in the brain tissue of DRPLA patients and compared it with that of recombinant ATN1 in COS-7 cells. We examined, postmortem, the brain tissues from a DRPLA patient whose DRPLA genes contained 63 and 15 CAG repeats. Total homogenate and a crude nuclear fraction were prepared from the DRPLA brain tissues, and were then examined by immunoblotting with C580R. Immunoblots of the total homogenate and the nuclear fraction showed an immunoreactive band at $\sim$ 140 kDa that corresponded to mF2 in COS-7 cells in addition to the mutant and wild-type, full-length ATN1s (Fig. 5A). Next, we examined the intracellular localization of ATN1 using the subcellular fractionation of the protein into the four fractions as described above. The mF2 fragment in the cerebellum of the DRPLA brain was demonstrated in the cytoplasmic membrane/organelle and insoluble fractions on the immunoblots by staining with C580R, L55-2 and 1C2 antibodies (Fig. 5B). We observed a single immunoreactive band of mF2 with an expanded polyQ but no other immunoreactive band for F2 with a normal sized polyQ from the DRPLA brain tissue. Using immunohistochemical staining with the ATN1 antibody, we noticed L55-2 labelled neuronal intranuclear and cytoplasmic inclusions in the affected lesion of the DRPLA brain tissues (Fig. 5C).

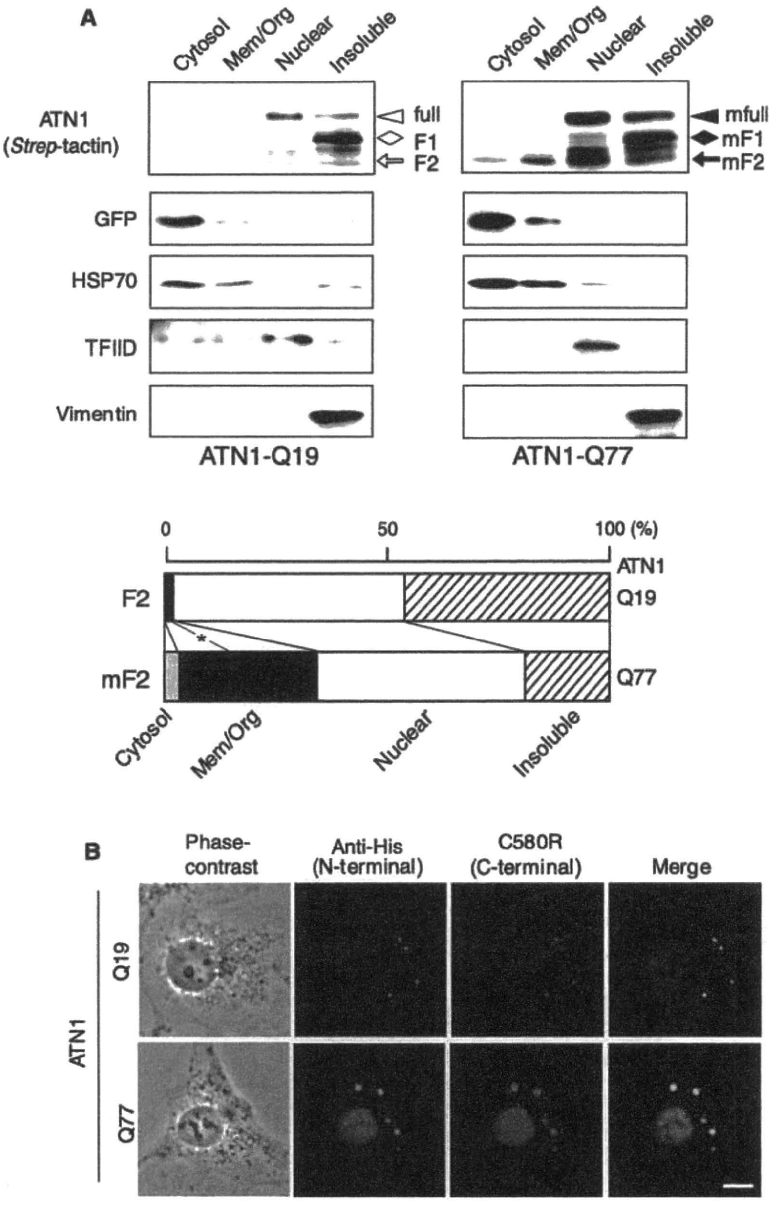

Fig. 4. Subcellular localization of ATN1-Q19 and -Q77 expressed in COS-7 cells. (A) After 48 h of transfection, the expressed cells were fractionated into cytosolic, membrane/organelle (Mem/Org), nuclear and insoluble fractions, in accordance with the protocol of the ProteoExtract subcellular proteome extraction kit. Western blotting showed that the full-length ATN1s (arrowheads) were detected in the nuclear and insoluble fractions, whereas F1 and mF1 were detected in the insoluble fraction (lozenges). Note that mF2 is found in the membrane/organelle, nuclear and insoluble fractions (black arrow). Stacked bar graphs present the ratio of distribution of F2 and mF2. Data are plotted from four independent experiments. $*P < 0.05$ (Student's *t*-test). To display the selectivity of subcellular fractions, marker proteins were immunoblotted with three antibodies: HSP70 for cytosolic, TFIID for nuclear and vimentin for insoluble fractions. Ten micrograms of protein were loaded per lane. Representative immunoblots of four independent experiments are shown. (B) Twenty-four hours after transfection with the ATN1-Q19 or -Q77 construct, COS-7 cells were visualized by immunofluorescence microscopy. Immunocytochemistry using His-tag (green) and C580R (red) antibodies shows that ATN1-Q19 and -Q77 were localized both in the cytoplasm and nucleus. The immunoreactivity of ATN1-Q77 was stronger than that of ATN1-Q19. Scale bar = 10 μm.

To clarify the proteolytic processing of ATN1 and understand its regulation, we treated the ATN1-expressing COS-7 cells with protease inhibitors, including caspase inhibitors, and assessed the resultant cell lysates by western blotting. When cells expressing ATN1-Q19 were treated with proteasome inhibitors, the blotting analysis showed that the amounts of the full-length ATN1 and F1 increased (Fig. 6A). Specific inhibitors of proteasomes (MG-132 and lactacystin) findings indicate that the ubiquitin-proteasome pathway is involved in the processing of ATN1, and the proteasome appears to primarily target the full-length ATN1. By contrast, when the cells were treated with caspase inhibitors, the blot membrane showed that the full-length ATN1 and F2 were increased by treatment with a pan-caspase inhibitor, benzyloxycarbonyl-Val-Ala-Asp(OMe)-fluoromethyl ketone (Z-VAD-FMK), although they were not increased by other selective

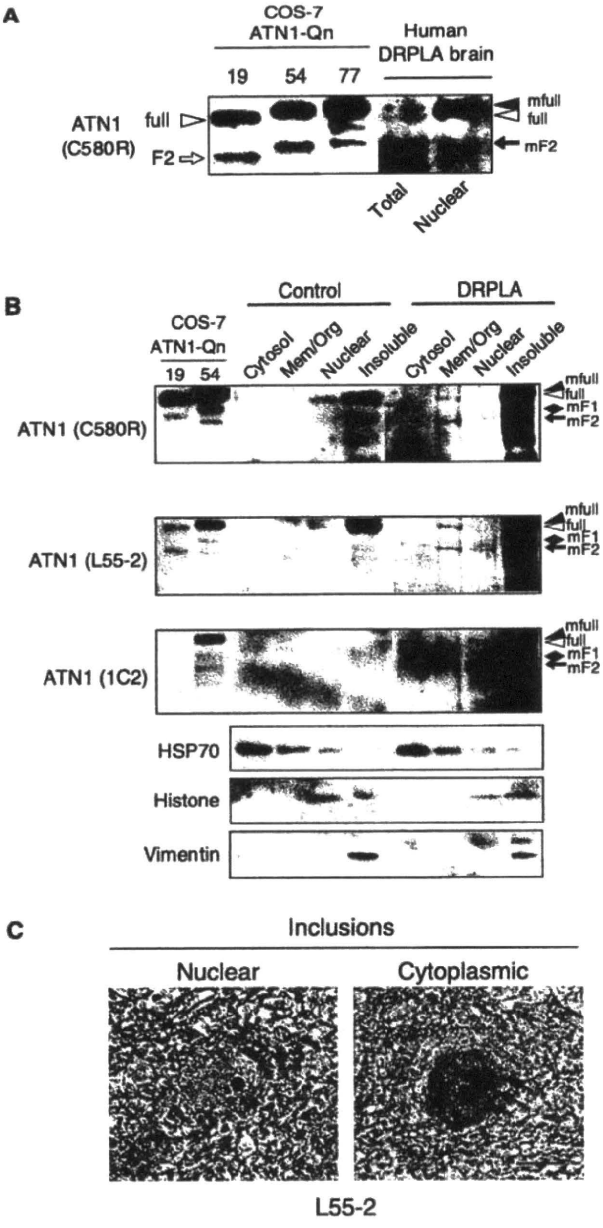

Fig. 5. Subcellular localization of ATN1 in the human DRPLA brain tissues. (A) Samples of COS-7 cells expressing ATN1-Q19, -Q54 and -Q77, and the cerebellum of a DRPLA patient were immunoblotted using C580R. Because the DRPLA patient had 63 and 15 CAG repeats on the DRPLA gene, ATN1-Q19, -Q54 and -Q77, were useful for comparison. The immunoblot showed that a single band of the mF2 fragment with expanded polyQ was specifically found in the DRPLA brain tissue (black arrow). (B) The human control and DRPLA brain tissues were fractionated into cytosolic, cytoplasmic membrane/organelle (Mem/Org), nuclear and insoluble fractions. To display the selectivity of subcellular fractions, marker proteins were immunoblotted with three antibodies: HSP70 for cytosolic, Histone H4 for nuclear and vimentin for insoluble fractions. ATN1 (C580R and L55-2) and polyQ antibodies detected the immunoreactivity of mF2 in the cytoplasmic membrane/organelle and insoluble fractions of the DRPLA brain tissues. Twenty micrograms of protein were loaded per lane. Representative immunoblots of three independent experiments are shown. (C) The brain tissues of the DRPLA patient were immunohistochemically stained with L55-2. L55-2-labelled neuronal nuclear (arrowhead) and cytoplasmic inclusions (arrows) in the dentate nucleus. Scale bar = 10 μm.

caspase inhibitors (Fig. 6B). COS-7 cells expressing ATN1 were also treated with metalloprotease inhibitors. The blots of cell lysates treated with *N*,*N*,*N*′,*N*′-tetrakis(2-pyridylmethyl)ethylenediamine (TPEN) showed an increase in the full-length ATN1 and F1, although those treated by other metalloprotease inhibitors showed no increase (Fig. 6C). When COS-7 cells expressing ATN1 were subjected to double treatment with two inhibitors, Z-VAD-FMK and TPEN, the blot showed that both F1 and F2 increased (Fig. S5A). Z-VAD-FMK selectively increased the signal intensity of F2. Thus, F1 and F2 were processed in different pathways. Western blots including cells treated with other protease inhibitors showed no increase of these bands (Fig. S5B). Although proteasome inhibitors and the zinc-dependent protease inhibitor were involved in the accumulation of the full-length ATN1 and F1, Z-VAD-FMK selectively induced the accumulation of the full-length ATN1 and F2 in COS-7 cells.

To investigate the effect of polyQ expansion on the proteolytic processing of ATN1, we also examined COS-7 cells expressing ATN1 with normal and expanded polyQ tract after treatment with protease inhibitors. Western blots containing cells treated with Z-VAD-FMK revealed that mF2 in ATN1-Q77 with treatment of Z-VAD-FMK displayed higher reactivity than that without the treatment, whereas the full-length ATN1 in ATN1-Q77 showed similar reactivity with and without the treatment (Figs 6D and S5A). These data indicated that polyQ expansion induced the accumulation of mF2 by inhibition of caspases. We further investigated how Z-VAD-FMK treatment influenced the subcellular distribution of ATN1 and its fragments, by performing immunocytochemical analysis to compare untreated and Z-VAD-FMK-treated cells. Cells treated with Z-VAD-FMK showed that the aggregation composed by the C-terminal fragments of ATN1 increased in the cytoplasm (Fig. 6E). Moreover, Z-VAD-FMK treatment decreased immunoreactivity in the nucleus, demonstrating a difference compared to cells expressing ATN1-Q77.

Discussion

One of the primary pathological processes underlying the neurodegeneration that occurs in DRPLA is

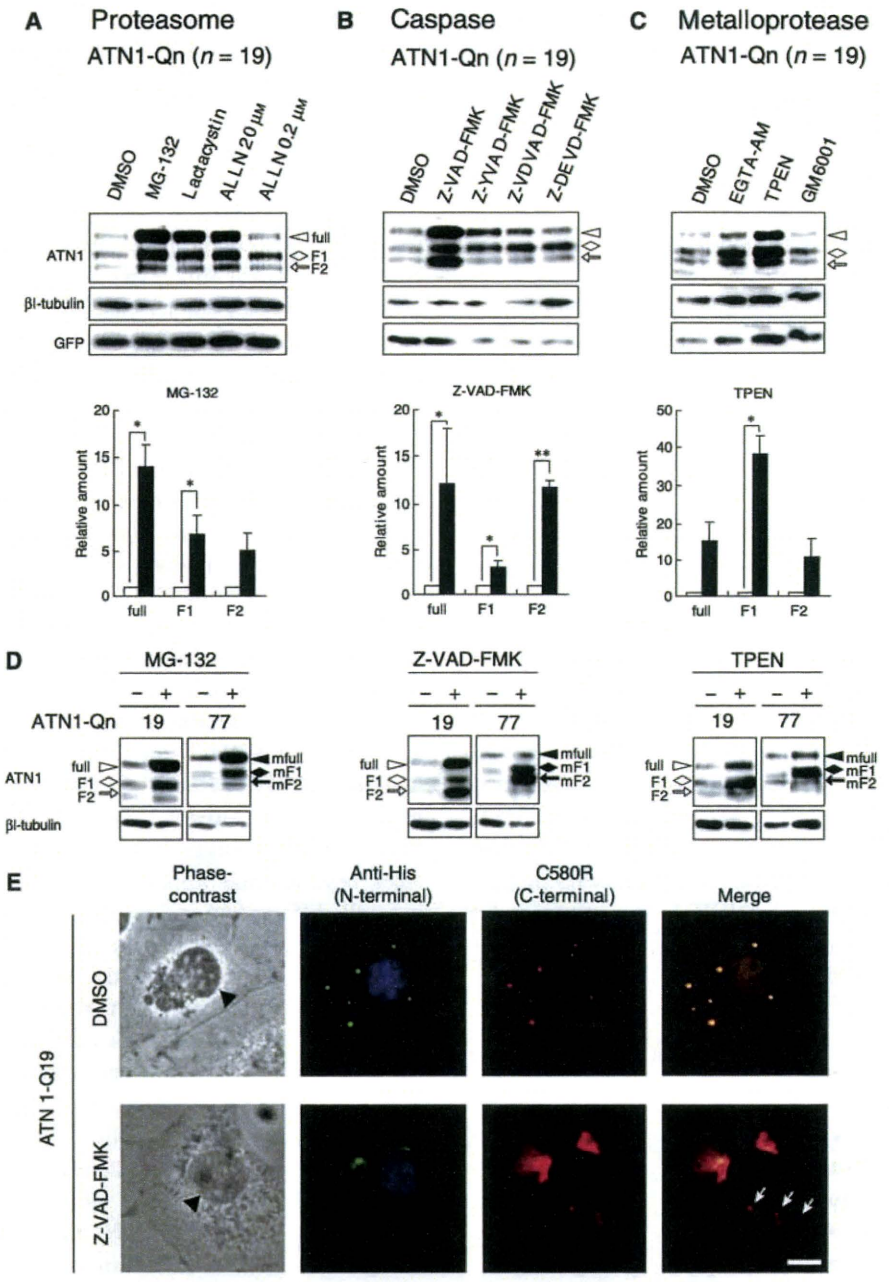

Fig. 6. Effect of protease inhibitors on ATN1-Q19 and -Q77 expressed in COS-7 cells. After 24 h of transfection, COS-7 cells expressing ATN1-Q19 were incubated for 24 h in serum-free medium with inhibitors: (A) proteasome and calpain inhibitors, MG-132 (10 μM), lactacystin (25 μM) and ALLN (20 μM, 0.2 μM); (B) caspase inhibitors, Z-VAD-FMK (50 μM for pan caspase), Z-YVAD-FMK (50 μM for caspase-1/4), Z-VDVAD-FMK (50 μM for caspase-2) and Z-DEVD-FMK (50 μM for caspase-3/6/7/10); and (C) metalloprotease inhibitors, EGTA-AM (50 μM for Ca^{2+}-dependent protease), TPEN (0.5 μM for Zn^{2+}-dependent protease) and GM6001 (50 μM for matrix metalloprotease). Western blotting showed that the reactivity of the C-terminal F2 fragment (white arrow) was increased by Z-VAD-FMK but was not significantly increased by the other inhibitors. Bar graphs include a quantitative analysis of ATN1s on the blots of COS-7 cells treatment with MG-132, TPEN and Z-VAD-FMK. $*P < 0.05$ and $**P < 0.01$ (Student's *t*-tests). (D) COS-7 cells expressing ATN1-Q19 and -Q77 were treated with MG-132, Z-VAD-FMK and TPEN. The mF2 fragment (black arrow) of ATN1-Q77 showed selectively increased reactivity after treatment with Z-VAD-FMK. (E) Twenty-four hours after treatment with Z-VAD-FMK and control dimethyl sulfoxide, COS-7 cells expressing ATN1-Q19 were visualized by immunofluorescence using His-tag (green) and C580R (red) antibodies. Immunocytochemistry showed that cytoplasmic aggregates of ATN1 C-terminal fragments were increased by Z-VAD-FMK treatment. Note that additional aggregates are labelled with C580R (red) in the cytoplasm of COS-7 cells with Z-VAD-FMK treatment (white arrows). The black arrowhead shows the nucleus. Scale bar = 10 μm.

nuclear accumulation of ATN1 and its cleaved fragments with polyQ expansion [17,24]. The details of the proteolytic processing of ATN1 remain unknown, whereas proteolysis of HD gene products (huntingtin) at the caspase-6 cleavage site was suggested to represent an initial event in the pathogenesis of HD [25]. In the present study, we aimed to elucidate some of details of the proteolytic processing of ATN1 and the mechanisms of ATN1 accumulation with the expansion of polyQ. We generated a cellular model of DRPLA, in which ATN1 and its fragments were accumulated in COS-7 cells expressing the *ATN1* gene by systematically increasing the number of polyQs expressed. We identified novel C-terminal fragments containing the polyQ tract in COS-7 and Neuro2a cells. ATN1 was processed into two C-terminal fragments that lost the nuclear localizing signal (NLS) in the N-terminal. One of the C-terminal fragments, F2, contained a polyQ tract; in addition, the mutant C-terminal fragment with an expanded polyQ tract (mF2) was specifically demonstrated in brain tissues from DRPLA patients. The increased amount of mF2 was likely caused by the pathological accumulation of ATN1, and was a result of the expansion of the polyQ tract. The present immunocytochemical study revealed that the accumulation of ATN1 and C-terminal fragments was localized in the cytoplasm and in the nucleus of cells. Indeed, the significant neuropathological features characterizing DRPLA are cytoplasmic inclusions, which are immunoreactive to ubiquitin and ATN1 antibodies, and also include nuclear inclusions in the DRPLA brains [2,26]. In the present study, the ATN1 antibody L55-2 labelled neuronal cytoplasmic and nuclear inclusions in the DRPLA brain. The biochemical examination of subcellular localization demonstrated that mF2 was preferentially localized in the cytoplasmic membrane/organelle and insoluble fractions, whereas the full-length ATN1 and the other C-terminal fragment were individually localized in the other fractions. Therefore, the proteolytic processing of ATN1 is likely to regulate the localization of C-terminal fragments. Moreover, a pan-caspase inhibitor selectively increased the accumulation of the C-terminal fragment in the cytoplasm, which recapitulated the cytoplasmic inclusion seen in the DRPLA brain. Taken together, these data suggest that the C-terminal fragment of ATN1 plays an important role in the accumulation of ATN1, ultimately leading to neurodegeneration in DRPLA.

Proteolytic processing of the gene products responsible for polyQ diseases has been shown to create toxic fragments containing expanded polyQ tracts *in vitro*, although whether all of the proteins undergo cleavage *in vivo* is unclear. Previous studies have determined that caspase acts as a catabolic enzyme that targets proteins with a polyQ tract. For example, Wellington *et al.* [20] predicted that cleavage sites for caspase were contained in huntingtin, ATN1, ataxin-3 and androgen receptor, and showed that the cleavage of all four proteins could be inhibited by treatment of caspase inhibitors. Other studies have shown that, in HD, the N-terminal huntingtin fragment that contains the polyQ tract was cleaved by caspase-3 *in vitro* and in the human brain tissues [27], and that cleavage at the caspase-6 site in huntingtin was essential for the HD-related behavioural and neuropathological features in the YAC128 model of HD [25]. Previous studies of DRPLA also showed that caspase-3 generated a C-terminal fragment containing the polyQ by cleavage at Asp109 *in vitro*, and that blocking the cleavage at Asp109 reduced aggregation of mutant ATN1 with expanded polyQ in 293T cells [19,21]. In the present study, however, we demonstrated that an inhibitor of caspase-3 activity produced no reduction in the accumulation of C-terminal F2 fragment. Interestingly, the general caspase inhibitor Z-VAD-FMK increased the accumulation of the C-terminal F2 fragment in the cellular model of DRPLA. Caspases, a family of cysteine proteases, are mostly activated in the cytoplasm. Recent findings suggest that caspases may have other roles beyond their apparent role in apoptosis, including cell differentiation, proliferation and other nonlethal events [28]. The importance of activated caspases has also been extended to the central nervous system, where proteases have been shown to contribute to axon guidance, synaptic plasticity and neuroprotection [29]. A recent study demonstrated that caspase-3 directly cleaved AMPA receptor subunit GluR1 and modulated neuronal excitability [30]. We speculate that the cleavage of ATN1 by caspases may be involved in the regulatory mechanism of ATN1. In particular, decelerated cleavage of ATN1 might induce disruption of signal transduction and consequently cause neurodegeneration. Further investigations are necessary to determine the specific type of caspases that process ATN1 and the role of caspases in ATN1 accumulation.

Previous immunohistochemical studies demonstrated that ATN1 localized in both the nucleus and cytoplasm of neurones in the human central nervous system [15,22,31]. The data obtained from the biochemical and immunocytochemical analyses of the present study demonstrated that the full-length ATN1 and C-terminal fragments localized in the nucleus and the cytoplasm in COS-7 cells. The sequence of ATN1 contains an NLS in the N-terminal and a nuclear

export signal in the C-terminal. Mutational assays demonstrated that these signals are functional in ATN1 and that deletion or mutation of the nuclear export signal in ATN1 changed its localization, whereby it accumulated in the nucleus and increased cellular toxicity [18]. The cleavage products F1 and F2 of ATN1 represent a failure of the N-terminal NLS to import the proteins into the nucleus. Thus, we predict that the complete, full-length ATN1 is imported into the nucleus and is subsequently cleaved into F1 and F2 (Fig. 7A). There is also evidence that F1 and F2 are processed individually in the nucleus (Fig. S5A). TPEN, which suppressed the degradation of F1, failed to induce a change in F2 accumulation. Conversely, the inhibition of the F2 degradation by Z-VAD-FMK failed to induce the accumulation of F1. Thus, we expect that the C-terminal fragments of ATN1 are processed via independent pathways (Fig. 7A). Moreover, a biochemical examination of the intracellular distribution of the C-terminal fragments demonstrated that the localization of F2 differed from that of F1. We assume that F2 is again exported to the cytoplasm as a nucleocytoplasmic shuttling protein and functions in the cytoplasm, whereas F1 stays in the nucleus and executes its function on the nuclear matrix. As previously demonstrated in the human DRPLA brain tissue [15], ATN1 assembles in the perinuclear cytoplasm where caspases can be activated to regulate the accumulation of the F2 fragment. Thus, the shuttling system of ATN1 may play an important role in DRPLA neurodegeneration. It is tempting to speculate that blocking caspase activity may also inhibit the shuttling system of ATN1, resulting in cytoplasmic accumulation of the ATN1 fragment and nuclear depletion of ATN1s (Fig. 7B).

The cellular models of DRPLA that were generated in the present study proved useful for further elucidation of the mechanisms of DRPLA neurodegeneration. Our models reproduced the pathological accumulation of the C-terminal fragment also observed in the DRPLA brain tissue. Moreover, the models demonstrated that the proteolytic processing of ATN1 regulated the intracellular localization of the cleaved fragments. Because the COS-7 and Neuro2a cellular models are able to demonstrate the accumulation of ATN1s in a much shorter period than that of DRPLA patient neuropathology, they are useful for analyzing the early stages of ATN1 accumulation with polyQ expansion. Using the cellular models, further experiments should be performed to reveal additional clues allowing exploration of a therapeutic target for neurodegeneration in DRPLA.

Experimental procedures

Construction of human ATN1 expression vector

The gene coding the full-length *ATN1* was amplified from Human Brain, cerebral cortex Marathon-Ready cDNA (Clontech, Palo Alto, CA, USA) with high-fidelity enzyme

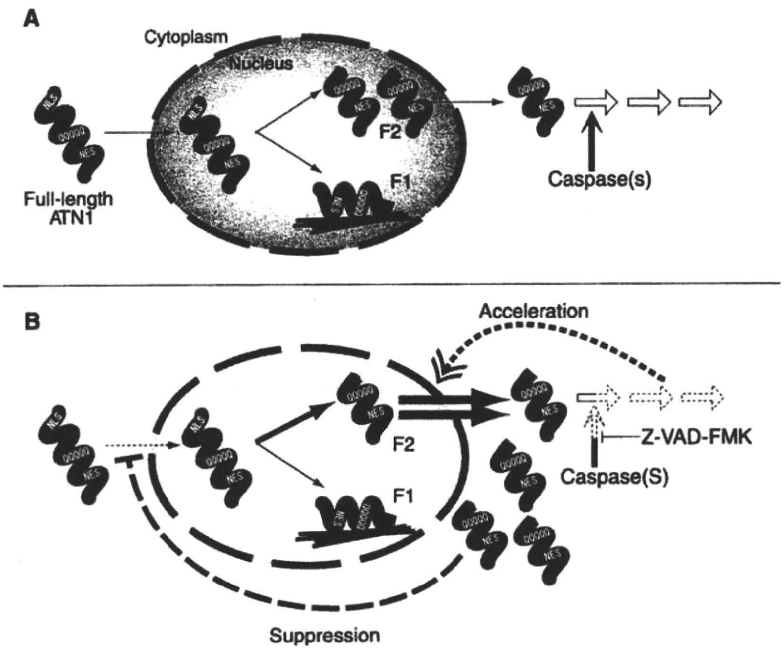

Fig. 7. (A) A schematic representation of a hypothetical model for proteolytic pathways of ATN1 in COS-7 cells. After importation into the nucleus, the full-length ATN is independently cleaved to F1 and F2 fragments. F1 stays within the nuclear matrix. F2 exports to the cytoplasm and assembles in the cytoplasmic organelle. Caspases are directly involved in the cleavage of F2, and regulate the accumulation of F2 in the cytoplasm. (B) When caspase activity is blocked by Z-VAD-FMK, the degradation of F2 is inhibited. This accelerates the accumulation of F2 in the cytoplasm and suppresses the nuclear transport of the full-length ATN1, which leads to the depletion of ATN1 and the fragments in the nucleus.

PrimeSTAR HS DNA polymerase (Takara Bio, Shiga, Japan) using the sequence specific primer by PCR and the product was cloned into pT7Blue (Novagen, San Diego, CA, USA). The resultant plasmid was designated as *ATN1*-pT7Blue. An *Xho*I restriction enzyme site was appended to Human *ATN1* at the 5′-end by PCR and changed vector to pRSETb (Invitrogen, Carlsbad, CA, USA) to yield a construct (*ATN1*-pRSET) in which the entire coding region of the gene is fused to a 6xHis-tag and a T7-tag at the 5′-region. To fuse a *Strep*-tag II sequence to the 3′-region of the *ATN1* gene, PCR was performed using the set of primers: forward, 5′-ATCGCAACCATCCATTCTACGTG-3′ and reverse, 5′-TTATTTTTCGAACTGCGGGTGGCTCC AAGCGCTCAGTGGCTTGTCGCTTTCCTTCTTCAGGT G-3′ (the *Strep*-tag II sequence is underlined) and with *ATN1*-pT7Blue as the template. The PCR product was digested with *Bsp*1407I and *Eco*RI, which was ligated with the product of *ATN1*-pRSET digestion by the same set of enzymes. The resultant plasmid was designated as *ATN1-St*-pRSET. Furthermore, for effective expression of fusion ATN1, expression vectors were changed to pcDNA3.1(+) (Invitrogen) and pET-30a(+) (Novagen) from pRSET. A *Hind*III restriction enzyme site was added *ATN1* on *ATN1-St*-pRSET at the 5′-end by PCR. The *ATN1* fragment containing the three tag sequences was cleaved from *ATN1-St*-pRSET, and then ligated into pcDNA3.1(+) or pET-30a(+) vectors. The expression vectors were termed *ATN1*-pcDNA3.1 and *ATN1*-pET30. All recombinant plasmids were introduced into *E. coli* JM109. The nucleotide sequences of all constructs were confirmed using dye terminator methods.

Transient expression of ATN1 in COS-7 and Neuro2a cells

COS-7 and Neuro2a cells were maintained in DMEM supplemented with 10% fetal calf serum. FuGENE 6 (Roche Diagnostics, Basel, Switzerland) was used for the introduction of exogenous DNA into COS-7 and Neuro2a cells in accordance with the manufacturer's instructions. Briefly, 1×10^5 cells were plated on 35 mm dishes and, 24 h later, each dish was transfected with 2 μg of *ATN1*-pcDNA3.1, 0.02 μg *EmGFP*-pcDNA3.1 and 6 μL of FuGENE6, and incubated at 37 °C for 48 h. Whole cell lysates were prepared with 20 mM HEPES-buffered saline (pH 7.4), 1% SDS (HBS-SDS) with protease inhibitors. To determine the molecular basis for increasing the amount of ATN1, the stability of ATN1-Q19 or -Q77 was examined by inhibition of protein synthesis. Forty-eight hours after transfection, the COS-7 cells were incubated with cycloheximide (100 $\mu g \cdot mL^{-1}$; Sigma-Aldrich, St. Louis, MO, USA). Cycloheximide interacts with the translocase enzyme and blocks protein synthesis in eukaryotic cells. The cells were then lysed after 0, 0.5, 1 or 2 h in HBS-SDS.

Subcellular protein extraction of COS-7 cells

Subcellular fractionation of COS-7 cells expressing ATN1s was performed using a ProteoExtract subcellular proteome extraction kit (Merck, Darmstadt, Germany) accordance with the manufacturer's instructions. Briefly, COS-7 cells (5×10^5 cells per 100 mm dish) were transfected with 10 μg of *ATN1-Q19-* or *-Q77*-pcDNA3.1, 0.1 μg of *EmGFP*-pcDNA3.1 and 27 μL of FuGENE6, and incubated at 37 °C for 48 h. After washing twice with ice-cold wash buffer, the cells were incubated with 1 mL of extraction buffer I at 4 °C for 10 min, and the supernatant was collected and used as the cytosolic fraction. The pellet was incubated with 1 mL of extraction buffer II at 4 °C for 30 min, and the supernatant was collected and used as the cytoplasmic membrane/organelle fraction. The pellet was incubated with 0.5 mL of extraction buffer III at 4 °C for 10 min, then the supernatant was used as the nuclear fraction, and the precipitate as the insoluble fraction.

Treatment with protease inhibitors

Twenty-four hours after transfection with *ATN1-Q19*-pcDNA3.1, the medium was replaced with serum-free medium, and then the cells were incubated with proteasome or protease inhibitors for 24 h. Cells were incubated with an equivalent amount of the vehicle, dimethyl sulfoxide as a control. The cells were treated with the proteasome inhibitors MG-132 (10 μM; Peptide Institute, Osaka, Japan), lactacystin (50 μM; Peptide Institute), calpain/proteasome inhibitor ALLN (0.2 μM and 20 μM; Roche Diagnostics), pan caspase inhibitor Z-VAD-FMK (50 μM; Peptide Institute), caspase-1 and -4 inhibitor Z-YVAD-FMK (50 μM; Bachem, Dübendorf, Switzerland), caspase-2 inhibitor Z-VDVAD-FMK (50 μM; BioVision, Mountain View, CA, USA), caspase-3, -6, -7 and -10 inhibitor Z-DEVD-FMK (50 μM; R&D Systems, Minneapolis, MN, USA), intracellular zinc chelator TPEN (0.5 μM; Sigma-Aldrich), intracellular calcium chelator EGTA-AM (50 μM; ABD Bioquest, Sunnyvale, CA, USA) and a broad-spectrum matrix metalloproteinase inhibitor GM6001 (50 μM; Merck). The cells were then assessed by western blotting and immunocytochemistry.

Expression of recombinant ATN1 in *E. coli*

The *ATN1*-pET30 was transformed into *E. coli* Rosetta2 (DE3)pLysS (Novagen)-competent cells. The Rosetta2 (DE3)pLysS strain is a BL21 derivative designed to alleviate codon bias when expressing heterologous proteins in *E. coli*, which supplies tRNAs for seven rare codons (AGA, AGG, AUA, CUA, GGA, CCC and CGG). The transformed *E. coli* was incubated overnight in 5 mL of LB culture medium containing kanamycin (50 $\mu g \cdot mL^{-1}$) and chloramphenicol (34 $\mu g \cdot mL^{-1}$) at 37 °C. After the addition of an aliquot of 100 μL of culture to 10 mL of the LB

culture medium containing kanamycin, the culture was incubated at 37 °C until A_{600} of 0.6 was reached. Expression of the ATN1 protein was induced by the addition of isopropyl thio-β-D-galactoside to a final concentration of 1 mM and incubation for 3 h at 37 °C. Cells were harvested by centrifugation at 1500 *g* for 10 min. Cell lysates were subjected to western blotting.

Assessment of ATN1-tag fusion proteins

ATN1-tag fusion proteins expressed by the COS-7 and *E. coli* cells were detected by western blotting using a *Strep*-tag II detection system. Samples (40 μg each) were electrophoresed in a 6% polyacrylamide gel. Proteins were transferred electrophoretically to a nitrocellulose membrane (GE Osmonics, Hopkins, MN, USA). The membranes were incubated in 5% BSA in NaCl/Tris (TBS) (pH 7.4). Then the membranes were incubated with Biotin Blocking Buffer (IBA, Göttingen, Germany) for 10 min, and *Strep*-tag II on ATN1 was visualized directly using *Strep*-Tactin HRP conjugate (dilution 1 : 5000; IBA) using an enhanced chemiluminescence reagent (ECL Plus; GE Healthcare, Little Chalfont, UK).

ATN1 antibodies

L55-2 is a polyclonal antibody raised against human ATN1. A synthetic peptide corresponding to human ATN1 residues 422-440 (NQPPKYTQPSLPSQAVWSQ) was conjugated with keyhole limpet hemocyanin and used to immunize rabbits. The antisera were purified by affinity chromatography. The resulting polyclonal antibody, L55-2, was used for immunoreactive probing. C580R is a polyclonal antibody raised against the C-terminus of human ATN1. C580R was reproduced according to a method that generated C580, as described previously [15]. 1C2 (Chemicon, Temecula, CA, USA) is a monoclonal antibody that recognizes polyQ tracts.

Immunoblotting

Protein concentrations were measured by bicinchoninic acid protein assay (Thermo Fisher Scientific, Waltham, MA, USA). Samples were electrophoresed in 6% polyacrylamide gel. The proteins were transferred to poly(vinylidene difluoride) (Atto, Tokyo, Japan). The poly(vinylidene difluoride) membranes were incubated in 5% nonfat milk powder in TBS, then they were incubated with monoclonal or polyclonal primary antibodies, followed by HRP-conjugated secondary antibodies. The antibodies used were: C580R (dilution 1 : 10 000), L55-2 (dilution 1 : 20 000), 1C2 (dilution 1 : 20 000), β-tubulin I monoclonal (dilution 1 : 10 000; Sigma-Aldrich), GFP monoclonal (Living Colors A.v. JL-8) (dilution 1 : 10 000; Clontech), TFIID polyclonal (dilution 1 : 5000; Santa Cruz Biotechnology, Santa Cruz, CA, USA), Histone H4 polyclonal (dilution 1 : 200; Cell Signaling Technology, Beverly, MA, USA), HSP70 monoclonal (dilution 1 : 5000; StressMarq Biosciences, Victoria, BC, Canada) and vimentin clone VIM 13.2 monoclonal (dilution 1 : 5000; Sigma-Aldrich). Immunoreactive proteins were visualized using an ECL Plus.

Immunocytochemistry

COS-7 cells (5×10^4) were plated on 35 mm dishes and, 24 h later, each dish was transfected. Twenty-four hours after transfection, the cells were fixed with 4% paraformaldehyde, and then incubated with monoclonal GFP antibody (dilution 1 : 500; Chemicon) and polyclonal C580R antibody (dilution 1 : 200), as described previously [32]. Alexa 488 anti-mouse IgG or Cy3-labelled anti-rabbit IgG was used as secondary antibodies. Nuclei of cells were visualized by staining with 4′-6-diamidino-2-phenylindole.

Preparation of human brain tissue samples

Post-mortem brain tissue samples from four DRPLA patients, whose diseases had been diagnosed genetically by PCR analysis and confirmed pathologically, and the brain tissue samples from control subjects were examined [15,22]. Tissue samples (1.0 g) from the cerebra and cerebella were homogenized separately in five volumes of TBS with protease inhibitors (20 mM Tris–HCl, pH 7.5, 150 mM NaCl, 1 $\mu g \cdot mL^{-1}$ aprotinin, 1 mM EDTA, 10 $\mu g \cdot mL^{-1}$ leupeptin, 0.5 mM pefabloc SC and 10 $\mu g \cdot mL^{-1}$ pepstatin). In the crude subcellular fractionation experiment, the tissue samples (1.0 g) were homogenated in five volumes of 0.32 M sucrose/50 mM Tris–HCl (pH7.4), as described previously [15]. The homogenates were centrifuged at 1000 *g* for 20 min, and the pellet (nuclear fraction) was resuspended with TBS with protease inhibitors. Next, subcellular fractionation of ATN1 in the control and DRPLA brain tissues was analyzed by the ProteoExtract subcellular proteome extraction kit as described for the subcellular protein extraction of COS-7 cells. For immunohistochemical studies, the human control and DRPLA brain tissues were fixed in 10% formalin and embedded in paraffin. The sections from the brain tissues were immunostained with ATN1 antibodies as described previously [15]. The experiments involving human subjects were undertaken with the understanding and written informed consent of each individual. The NCGG Institutional Review Board approved the experiments involving human subjects.

Acknowledgements

We thank Keiko Tsuzuku for technical assistance. This work was supported by the Research Funding for Longevity Sciences (21A-3) from National Center for

Geriatrics and Gerontology (NCGG); a Grant-in-Aid for Research on Intractable Diseases from the Ministry of Health, Labor and Welfare, Japan; and Okinaka Memorial Institute for Medical Research.

References

1 Zoghbi HY & Orr HT (2000) Glutamine repeats and neurodegeneration. *Annu Rev Neurosci* **23**, 217–247.

2 Yazawa I (2003) Pathological mechanism of neurodegeneration in polyglutamine diseases. In *Recent Research Developments in Biophysics and Biochemistry*, Vol. 3 (Pandalai SG ed.), pp. 21–28. Research Signpost, India.

3 Orr HT & Zoghbi HY (2007) Trinucleotide repeat disorders. *Annu Rev Neurosci* **30**, 575–621.

4 Ross CA & Poirier MA (2004) Protein aggregation and neurodegenerative disease. *Nat Med* **10**(Suppl.), S10–S17.

5 Klement IA, Skinner PJ, Kaytor MD, Yi H, Hersch SM, Clark HB, Zoghbi HY & Orr HT (1988) Ataxin-1 nuclear localization and aggregation: role in polyglutamine-induced disease in SCA1 transgenic mice. *Cell* **95**, 41–53.

6 Saudou F, Finkbeiner S, Devys D & Greenberg ME (1998) Huntingtin acts in the nucleus to induce apoptosis but death does not correlate with the formation of intranuclear inclusions. *Cell* **95**, 55–66.

7 Kim M, Lee HS, LaForet G, McIntyre C, Martin EJ, Chang P, Kim TW, Williams M, Reddy PH, Tagle D *et al.* (1999) Mutant huntingtin expression in clonal striatal cells: dissociation of inclusion formation and neuronal survival by caspase inhibition. *J Neurosci* **19**, 964–973.

8 Arrasate M, Mitra S, Schweitzer ES, Segal MR & Finkbeiner S (2004) Inclusion body formation reduces levels of mutant huntingtin and the risk of neuronal death. *Nature* **431**, 805–810.

9 Ross CA (2002) Polyglutamine pathogenesis: emergence of unifying mechanisms for Huntington's disease and related disorders. *Neuron* **35**, 819–822.

10 Smith JK, Gonda VE & Malamud N (1958) Unusual form of cerebellar ataxia; combined dentato-rubral and pallido-Luysian degeneration. *Neurology* **8**, 205–209.

11 Naito H & Oyanagi S (1982) Familial myoclonus epilepsy and chroreoathetosis: hereditary dentatorubral-pallidoluysian atrophy. *Neurology* **32**, 798–807.

12 Takahashi H, Ohama E, Naito H, Takeda S, Nakashima S, Makifuchi T & Ikuta F (1988) Hereditary dentatorubral-pallidoluysian atrophy: clinical and pathological variants in family. *Neurology* **38**, 1065–1070.

13 Sano A, Yamauchi N, Kakimoto Y, Komure O, Kawai J, Hazama F, Kuzume K, Sano N & Kondo I (1994) Anticipation in hereditary dentatorubral-pallidoluysian atrophy. *Hum Genet* **93**, 699–702.

14 Burke JR, Wingfield MS, Lewis KE, Roses AD, Lee JE, Hulette C, Pericak-Vance MA & Vance JM (1994) The Haw River syndrome: dentatorubropallidoluysian atrophy (DRPLA) in an African-American family. *Nat Genet* **7**, 521–524.

15 Yazawa I, Nukina N, Hashida H, Goto J, Yamada M & Kanazawa I (1995) Abnormal gene product identified in hereditary dentatorubral-pallidoluysian atrophy (DRPLA) brain. *Nat Genet* **10**, 3–4.

16 Igarashi S, Koide R, Shimohata T, Yamada M, Hayashi Y, Takano H, Date H, Oyake M, Sato T, Sato A *et al.* (1998) Suppression of aggregate formation and apoptosis by transglutaminase inhibitors in cells expressing truncated DRPLA protein with an expanded polyglutamine stretch. *Nat Genet* **18**, 111–117.

17 Schilling G, Wood JD, Duan K, Slunt HH, Gonzales V, Yamada M, Cooper JK, Margolis RL, Jenkins NA, Copeland NG *et al.* (1999) Nuclear accumulation of truncated atrophin-1 fragments in a transgenic mouse model of DRPLA. *Neuron* **24**, 275–286.

18 Nucifora FC Jr, Ellerby LM, Wellington CL, Wood JD, Herring WJ, Sawa A, Hayden MR, Dawson VL, Dawson TM & Ross CA (2003) Nuclear localization of a non-caspase truncation product of atrophin-1, with an expanded polyglutamine repeat, increases cellular toxicity. *J Biol Chem* **278**, 13047–13055.

19 Miyashita T, Okamura-Oho Y, Mito Y, Nagafuchi S & Yamada M (1997) Dentatorubral pallidoluysian atrophy (DRPLA) protein is cleaved by caspase-3 during apoptosis. *J Biol Chem* **272**, 29238–29242.

20 Wellington CL, Ellerby LM, Hackam AS, Margolis RL, Trifiro MA, Singaraja R, McCutcheon K, Salvesen GS, Propp SS, Bromm M *et al.* (1998) Caspase cleavage of gene products associated with triplet expansion disorders generates truncated fragments containing the polyglutamine tract. *J Biol Chem* **273**, 9158–9167.

21 Ellerby LM, Andrusiak RL, Wellington CL, Hackam AS, Propp SS, Wood JD, Sharp AH, Margolis RL, Ross CA, Salvesen GS *et al.* (1999) Cleavage of atrophin-1 at caspase site aspartic acid 109 modulates cytotoxicity. *J Biol Chem* **274**, 8730–8736.

22 Yazawa I, Hazeki N & Kanazawa I (1998) Expanded glutamine repeat enhances complex formation of dentatorubral-pallidoluysian atrophy (DRPLA) protein in human brains. *Biochem Biophys Res Commun* **250**, 22–26.

23 Knight SP, Richardson MM, Osmand AP, Stakkestad A & Potter NT (1997) Expression and distribution of the dentatorubral-pallidoluysian atrophy gene product (atrophin-1/drplap) in neuronal and non-neuronal tissues. *J Neurol Sci* **146**, 19–26.

24 Shimohata T, Nakajima T, Yamada M, Uchida C, Onodera O, Naruse S, Kimura T, Koide R, Nozaki K, Sano Y *et al.* (2000) Expanded polyglutamine stretches

interact with TAFII130, interfering with CREB-dependent transcription. *Nat Genet* **26**, 29–36.
25 Graham RK, Deng Y, Slow EJ, Haigh B, Bissada N, Lu G, Pearson J, Shehadeh J, Bertram L, Murphy Z *et al.* (2006) Cleavage at the caspase-6 site is required for neuronal dysfunction and degeneration due to mutant huntingtin. *Cell* **125**, 1179–1191.
26 Yazawa I, Nakase H & Kurisaki H (1999) Abnormal dentatorubral-pallidoluysian atrophy (DRPLA) protein complex is pathologically ubiquitinated in DRPLA brains. *Biochem Biophys Res Commun* **260**, 133–138.
27 Kim YJ, Yi Y, Sapp E, Wang Y, Cuiffo B, Kegel KB, Qin ZH, Aronin N & DiFiglia M (2001) Caspase 3-cleaved N-terminal fragments of wild-type and mutant huntingtin are present in normal and Huntington's disease brains, associate with membranes, and undergo calpain-dependent proteolysis. *Proc Natl Acad Sci USA* **98**, 12784–12789.
28 Lamkanfi M, Festjens N, Declercq W, Vanden Berghe T & Vandenabeele P (2007) Caspases in cell survival, proliferation and differentiation. *Cell Death Differ* **14**, 44–55.
29 McLaughlin B (2004) The kinder side of killer proteases: caspase activation contributes to neuroprotection and CNS remodeling. *Apoptosis* **9**, 111–121.
30 Lu C, Fu W, Selvesen GS & Mattson MP (2002) Direct cleavage of AMPA receptor subunit GluR1 and suppression of AMPA currents by caspase-3. *Neuromolecular Med* **1**, 69–79.
31 Yamada M, Tan CF, Inenaga C, Tsuji S & Takahashi H (2004) Sharing of polyglutamine localization by the neuronal nucleus and cytoplasm in CAG-repeat diseases. *Neuropathol Appl Neurobiol* **30**, 665–675.
32 Hashimoto N, Murase T, Kondo S, Okuda A & Inagawa-Ogashiwa M (2004) Muscle reconstitution by muscle satellite cell descendants with stem cell-like properties. *Development* **131**, 5481–5490.

Supporting information

The following supplementary material is available:
Fig. S1. Generation of an increased number of CAG repeats.
Fig. S2. Expression of ATN1-Q19 and -Q77 in COS-7 and Neuro2a cells.
Fig. S3. Intracellular distribution of ATN1 in COS-7 cells.
Fig. S4. TUNEL assay of mammalian cell expressed ATN1-Q19 and -Q77.
Fig. S5. Effect of other protease inhibitors on expressed full-length ATN1 and fragments in COS-7 cells.

This supplementary material can be found in the online version of this article.

Please note: As a service to our authors and readers, this journal provides supporting information supplied by the authors. Such materials are peer-reviewed and may be re-organized for online delivery, but are not copy-edited or typeset. Technical support issues arising from supporting information (other than missing files) should be addressed to the authors.

EXPERIMENTAL CELL RESEARCH 317 (2011) 221–233

available at www.sciencedirect.com

ScienceDirect

www.elsevier.com/locate/yexcr

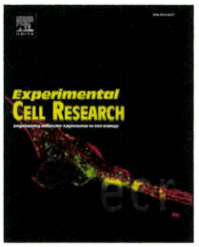

Research Article

Community effect triggers terminal differentiation of myogenic cells derived from muscle satellite cells by quenching Smad signaling

Michiko Yanagisawa[a,b,1], *Atsushi Mukai*[a,1], *Kosuke Shiomi*[a], *Si-Yong Song*[c], *Naohiro Hashimoto*[a,*]

[a]*Department of Regenerative Medicine, National Institute for Longevity Sciences, National Center for Geriatrics and Gerontology, 35 Gengo, Morioka, Oobu, Aichi 474-8522, Japan*

[b]*Aging Research, Nagoya University Graduate School of Medicine, 65 Tsurumai-cho, Showa-ku, Nagoya, Aichi 466-8550, Japan*

[c]*Institute of Neuroscience, Faculty of Pharmaceutical Sciences at Kagawa, Tokushima Bunri University, 1314-1 Shido, Sanuki-shi, Kagawa 769-2193, Japan*

ARTICLE INFORMATION

Article Chronology:
Received 18 April 2010
Revised version received
16 September 2010
Accepted 13 October 2010
Available online 20 October 2010

Keywords:
Community effect
BMP
Smad
ALK
Myogenesis
Osteogenesis

ABSTRACT

A high concentration of bone morphogenetic proteins (BMPs) stimulates myogenic progenitor cells to undergo heterotopic osteogenic differentiation. However, the physiological role of the Smad signaling pathway during terminal muscle differentiation has not been resolved. We report here that Smad1/5/8 was phosphorylated and activated in undifferentiated growing mouse myogenic progenitor Ric10 cells without exposure to any exogenous BMPs. The amount of phosphorylated Smad1/5/8 was severely reduced during precocious myogenic differentiation under the high cell density culture condition even in growth medium supplemented with a high concentration of serum. Inhibition of the Smad signaling pathway by dorsomorphin, an inhibitor of Smad activation, or noggin, a specific antagonist of BMP, induced precocious terminal differentiation of myogenic progenitor cells in a cell density-dependent fashion even in growth medium. In addition, Smad1/5/8 was transiently activated in proliferating myogenic progenitor cells during muscle regeneration in rats. The present results indicate that the Smad signaling pathway is involved in a critical switch between growth and differentiation of myogenic progenitor cells both in vitro and in vivo. Furthermore, precocious cell density-dependent myogenic differentiation suggests that a community effect triggers the terminal muscle differentiation of myogenic cells by quenching the Smad signaling.

Introduction

Signaling molecules have both permissive and repressive effects on gene expression in the myotomes during embryonic myogenesis. Skeletal muscle formation in the paraxial mesoderm is controlled by a number of signaling molecules emanating from neighboring tissues. Sonic hedgehog (Shh) and Wnt promote myogenesis [1]. In contrast, bone morphogenetic protein 4 (BMP4) inhibits premature differen-

* *Corresponding author.* Fax: +81 562 46 8464.
E-mail address: nao@ncgg.go.jp (N. Hashimoto).

Abbreviations: BMP, bone morphogenetic protein; ALK, activin-like kinase; MyHC, myosin heavy chain; BPV, bupivacaine hydrochloride

[1] These authors equally contributed to this study.

0014-4827/$ – see front matter © 2010 Elsevier Inc. All rights reserved.
doi:10.1016/j.yexcr.2010.10.011